

# Optimal monitoring design for uncertainty quantification during geologic CO<sub>2</sub> sequestration: A machine learning approach

Misael M. Morales<sup>a,b,\*</sup>, Mohamed Mehana<sup>a</sup>, Carlos Torres-Verdín<sup>b,c</sup>, Michael J. Pyrcz<sup>b,c</sup> and Bailian Chen<sup>a</sup>

<sup>a</sup>Earth and Environmental Sciences Division, Los Alamos National Laboratory, Los Alamos, NM 87544, USA

<sup>b</sup>Cockrell School of Engineering, The University of Texas at Austin, Austin, TX 78712, USA

<sup>c</sup>Jackson School of Geosciences, The University of Texas at Austin, Austin, TX 78712, USA

## ARTICLE INFO

### Keywords:

Geologic carbon sequestration  
Monitoring design optimization  
Machine learning  
Reduced-order modeling  
Data assimilation  
Uncertainty quantification

## ABSTRACT

An effective monitoring design is crucial to ensure the safe and permanent geologic storage of CO<sub>2</sub>. Optimal monitoring design involve an optimal placement of monitoring wells, and optimal monitoring measurement data (pressure, CO<sub>2</sub> saturation, temperature, etc.). We developed a filtering-based data assimilation approach to design an optimal monitoring strategy for well placement and monitoring data design. To efficiently solve the optimization problem and reduce computational costs, Artificial Neural Networks are used to develop computationally efficient reduced-order models based on full-physics numerical simulations of CO<sub>2</sub> injection in saline aquifers. We demonstrate our approach in two scenarios of CO<sub>2</sub> leakage through legacy or abandoned wellbores where an optimal monitoring strategy are devised to reduce the uncertainty in cumulative CO<sub>2</sub> leakage in the geologic CO<sub>2</sub> sequestration (GCS) site. The optimal monitoring design resulted in an uncertainty reduction in the cumulative leakage of CO<sub>2</sub> of approximately 73% and 62% in each case, respectively. The proposed approach is efficient in developing monitoring designs under geologic uncertainty and enables safe geologic carbon sequestration operations.


## 1. Introduction

Geologic CO<sub>2</sub> sequestration (GCS) has emerged as an important technology to reduce anthropogenic greenhouse gas emissions to the atmosphere [1, 2]. This has become increasingly popular worldwide due to the need to meet international climate protection agreements [3]. Different types of underground formations have been proposed to store CO<sub>2</sub> emissions including oil and gas reservoirs, coal beds and seams, and deep saline aquifers [4]. One of the main concerns in GCS projects is potential leakage of the CO<sub>2</sub> through leakage pathways, such as improperly abandoned wells, faults, and fractures [5, 6]. Such risks can pose a major threat to overlying resources (e.g., groundwater resources, oil and gas reservoirs, etc.) and human health [7]. Monitoring and verifying CO<sub>2</sub> behavior within the subsurface reservoir are crucial for detecting potential leakage, assessing storage capacity, and evaluating environmental impacts [8].

To ensure safe and efficient operations in a large-scale GCS site, risk management techniques are used to minimize and mitigate potential risks during CO<sub>2</sub> injection and post-injection periods [9, 10]. Monitoring is thus an important aspect of GCS risk management, which is one of the main goals of the Department of Energy (DOE) Office of Fossil Energy National Risk Assessment Partnership (NRAP) [11]. For this goal, several monitoring and carbon management techniques have been developed, including near surface CO<sub>2</sub> flux and tracer measurements [12], groundwater chemistry monitoring [13], seismic surveying [14], and pressure monitoring [15, 16].

Optimal sensor placement and monitoring design play a critical role in achieving accurate and efficient monitoring in GCS projects. Depending on the reservoir properties and heterogeneity, the placement of monitoring wells can provide a more accurate measurement of the injected CO<sub>2</sub> plume and help mitigate potential leakage risks [17, 18]. In common GCS operations, each injection well is paired with one monitoring well, though large-scale projects often incorporate a larger number of monitoring wells [19]. Moreover, the selection of monitoring measurement plays an

\*Corresponding author

 misaelmorales@utexas.edu (M.M. Morales)  
ORCID(s): 0000-0001-6923-1032 (M.M. Morales)

important role in reducing uncertainties and quantifying risks in GCS operations [20, 21]. Therefore, it is crucial to define an optimal monitoring strategy in terms of both well placement and monitoring measurement type.

Recent advancement in monitoring systems such as smart or intelligent wells are capable of providing large amounts of data in terms of volume, velocity, variety, value, and veracity [22]. Classical techniques in data processing and forecasting are sometimes hindered by big data, therefore machine learning provides a promising approach to enhance data-driven subsurface energy resource systems [23, 24]. By analyzing extensive data sets, machine learning algorithms can uncover complex latent patterns and relationships that may not be discernible through traditional methods [25, 26]. Machine learning approaches, when combined with reduced-order modeling (ROM) techniques, enable efficient and accurate prediction of key parameters, including pressure distribution and CO<sub>2</sub> plume migration [27, 28]. These insights facilitate the optimization of sensor placement and monitoring strategies, enabling better decision making and forecasting in GCS projects.

Accurately quantifying uncertainties is vital for the reliability of predictions and optimizing monitoring design under uncertain conditions [17, 29, 30]. Uncertainty quantification is particularly important in GCS due to inherent complexities and variabilities associated with subsurface conditions, fluid flow, and measurement errors [20, 31]. Several approaches for history matching or data assimilation have been applied to subsurface flow and transport, including Markov Chain Monte Carlo (MCMC) [25, 30, 32], randomized maximum likelihood (RML) [33], filter-based or rejection sampling (RS) [34], ensemble Kalman filtering (EnKF) [35] and ensemble smoother with multiple data assimilation (ES-MDA) [20, 36]. Filter-based approaches provide a robust framework for characterizing uncertainties associated with reservoir properties, operating conditions, and measurement errors, and with reduced complexity and cost compared to previously-mentioned techniques. Leveraging data assimilation techniques allows for informed risk assessment, ensuring the safety and efficiency of GCS projects.

Numerous research endeavors have been dedicated to addressing monitoring design, sensor placement, and uncertainty quantification in GCS. Previous studies have explored various modeling techniques, simulation frameworks, and optimization algorithms to enhance monitoring strategies and improve forecasting.

Efforts have been made to select the optimal monitoring measurements for GCS projects. Yonkofski et al. [37] use a simulated annealing (SA) global optimization approach to obtain the optimal monitoring measurement design in a GCS project. Their objective is to minimize the estimated time to first detection (ETFD) by iteratively mutating potential monitoring designs. Oladyskhin et al. [38] propose a polynomial chaos expansion (PCE) and bootstrap filtering approach for assimilating pressure data into reservoir models and quantifying the uncertainty reduction in CO<sub>2</sub> leakage rate at a GCS site. Liu and Grana [39] propose a deep convolutional autoencoder as a ROM strategy to assimilate seismic monitoring data in GCS. Their method requires high-fidelity simulations (HFS) to obtain CO<sub>2</sub> saturation plume predictions from an ensemble of prior models, which is then used to calculate the seismic response. The autoencoder is used to project the observed monitoring measurements into latent space, where ES-MDA is used to update the model parameters and quantify the uncertainty in predictions.

Similar efforts have been made in the area of optimal monitoring well placement. Sun et al. [21] propose an approach to optimize monitoring well location based on pressure measurements for GCS under geologic uncertainty. Using binary integer programming problem (BIPP) formulation, they effectively select optimal monitoring locations for homogeneous and fluvial heterogeneous reservoirs. However, their method requires a large number of forward simulations, which can be computationally costly and time consuming. Sun and Durlofsky [17] use a data-space inversion (DSI) approach to optimize the monitoring well locations in a GCS project with a genetic algorithm (GA) global optimization. Using principal component analysis (PCA) as a model reduction strategy, they reduce the uncertainty in CO<sub>2</sub> saturation plume using a RML approach. In this approach, posterior geological models are not generated in the DSI method, which is different from traditional ensemble-based data assimilation approaches.

Besides optimal well placement and monitoring measurement selection, several research studies have been conducted to quantify the uncertainty in GCS projects. Jia et al. [31] propose a Bayesian model average and Monte Carlo simulation to quantify parameter uncertainty based on a polynomial chaos expansion ROM. However, Monte Carlo strategies require a very large number of realizations and are extremely computationally inefficient. Chen et al. [20] propose a risk assessment approach using ES-MDA with geometric inflation factors (ES-MDA-GEO) to quantify the uncertainty monitoring data and calibrate the prior uncertain geologic models. Their work leverages continuous data assimilation as new monitoring data becomes available in GCS projects to improve the underlying model and reduce uncertainties. Mehana et al. [40] provide a ROM-based approach to quantify wellbore leakage from depleted reservoirs in CO<sub>2</sub>-EOR operations. They compare the performance of different machine learning-based ROMs for prediction of cumulative leakage and quantify the uncertainty using Monte Carlo simulations. Pawar et al. [41] provide a robust

framework for quantitative risk assessment of leakage in GCS. Utilizing the NRAP-open-IAM (Integrated Assessment Model) tool, they are able to quantify the leakage risk through legacy or abandoned wells in large-scale GCS projects. This framework can then be used to support permit applications for GCS projects.

In this paper, we build upon the work of Chen et al. [42] to systematically design an optimal monitoring placement and measurement strategy for large-scale GCS beyond naive monitoring well placement and monitoring design. Chen et al. [42] developed a robust framework for uncertainty reduction in cumulative CO<sub>2</sub> using Multivariate Adaptive Regression Splines (MARS) [43]. Furthermore, Chen et al. [42] use a filter-based data assimilation process to quantify the uncertainty reduction in cumulative CO<sub>2</sub> leakage. However, their work assumes a predetermined, uninformed placement of the monitoring well and monitoring measurement type, relying solely on engineering judgement and fixed monitoring configurations.

We propose a method for optimal GCS monitoring design based on well placement optimization and monitoring measurement selection, extending the work of Chen et al. [42] beyond fixed monitoring well locations and monitoring measurement type. We improve the ROM for flow simulation by implementing a more accurate and efficient artificial neural network (ANN) instead of MARS to predict cumulative CO<sub>2</sub> leakage from a prior ensemble of uncertain model parameters. Using the ANN ROM, we perform data assimilation using a filter-based approach to select the most informative monitoring well location and measurement type in order to reduce uncertainties in CO<sub>2</sub> leakage risks. Using the ANN ROM and the filter-based data assimilation, we implement an optimization loop to estimate the best monitoring well location and measurement type to reduce the uncertainty in CO<sub>2</sub> leakage. The structure of this paper is as follows: Section 2 present our methodology, Section 3 presents the results of our approach for two synthetic cases, and Section 4 summarizes our findings, discusses their implications, and outlines potential avenues for future research in the field of GCS.

## 2. Methodology

In this section we will discuss the approaches for uncertainty quantification, ROM development, reduced-order model training and performance, and optimal monitoring workflow design.

### 2.1. Uncertainty Quantification

Our goal is to evaluate the value of data in GCS monitoring design, which is quantified by the amount of uncertainty that is reduced in the cumulative CO<sub>2</sub> leakage,  $M_c$ , over the duration of a GCS project. The prior probability density function (PDF) of the cumulative CO<sub>2</sub> leakage is denoted as  $P(M_c)$ , where the prior refers to the probability distribution before a monitoring program is implemented. The distribution of potential monitoring data that could be measured at the monitoring wells is denoted as  $D = [d_1, d_2, \dots, d_{n_d}]$ , where  $\{d_i\}_{i=1}^{n_d}$  are the individual monitoring data points obtained if a monitoring design were implemented in a particular leakage scenario, and  $n_d$  is the total number of monitoring data points in  $D$ . Monitoring data is sampled monthly, and can represent pressure, CO<sub>2</sub> saturation, and/or temperature values at the monitoring well. Thus, we denote  $D^j$  as the  $j^{th}$  realization of  $D$ . For each  $D^j$ , we obtain a posterior PDF denoted by  $P(M_c|D^j)$ , which is calculated using a data assimilation procedure as the cumulative CO<sub>2</sub> leakage,  $M_c$ , for a given monitoring design data  $D^j$ . The objective is to quantify the value of information (VOI) estimated from a distribution of potential monitoring design, allowing us to choose an optimal monitoring well placement and monitoring measurement type to minimize the uncertainty in potential leakage scenarios.

Following Chen et al. [30, 42] and Le and Reynolds [44], the VOI is quantified by the uncertainty reduction in the objective function. We denote the amount of uncertainty in cumulative CO<sub>2</sub> leakage distribution  $P(M_c)$  as  $U[P(M_c)]$ , defined as:

$$U[P(M_c)] = P_{90}[P(M_c)] - P_{10}[P(M_c)], \quad (1)$$

where  $P_{10}[\bullet]$  is the 10<sup>th</sup> percentile of a distribution and  $P_{90}[\bullet]$  is the 90<sup>th</sup>. The distribution of cumulative CO<sub>2</sub> leakage is attributed to the uncertainty in model parameters, in this case the number of and the vertical transmissibility of potential leaky pathways,  $k_v^\ell$ , and the reservoir permeability multiplier,  $k_R$ . Therefore, selecting a monitoring design that reduces the uncertainty in  $M_c$  ensures that the monitoring design will function effectively under multiple possible potential leakage scenarios.

The expected posterior uncertainty distribution in  $M_c$  given  $D$  is given by:

$$E_d[U[P(M_c|D)]] = \frac{1}{\ell_d} \sum_{j=1}^{\ell_d} U[P(M_c|D^j)], \quad (2)$$

where  $E_d$  is the expectation with respect to all realizations of  $D$  and  $l_d$  is the number of data realizations. The expected uncertainty reduction,  $U_R$ , as a result of data acquisition from a potential monitoring design is given by the difference between the prior uncertainty and the expected posterior uncertainty in cumulative  $\text{CO}_2$  leakage, as defined by:

$$U_R = U[P(M_c)] - E_d[U[P(M_c|D)]]. \quad (3)$$

The optimal monitoring design is obtained by selecting the optimal monitoring well placement and monitoring measurement type in terms of uncertainty reduction,  $U_R$ . The uncertainty reduction,  $U_R$ , quantifies the effectiveness of the particular GCS monitoring design, where the higher the uncertainty reduction, the higher the VOI in the monitoring data location and type obtained in the monitoring design.

## 2.2. Reduced-Order Model Development

Given the computational cost of traditional filter-based data assimilation, a reduced-order model (ROM) is developed. The workflow for the ROM development is illustrated in Fig.1. This section provides a summary of the main steps in the ROM development workflow:

- Step 1. *Experimental design*: Given a set of uncertain parameters  $k_v^{\ell_d}$  and  $k_R$ , we generate  $n_s$  training samples using Latin Hypercube Sampling (LHS) [45].
- Step 2. *Forward simulations*: Physics-based high-fidelity simulation of  $\text{CO}_2$  injection and post-injection migration is performed with each of the  $n_s$  training samples using the Finite Element Heat and Mass Transfer (FEHM) simulator [46].
- Step 3. *Collect training data*: For each training realization, the set of uncertain parameters, monitoring data, and cumulative  $\text{CO}_2$  leakage are collected. The uncertain parameters are predictor inputs for the ROM training and the objectives of interest (cumulative  $\text{CO}_2$  leakage and monitoring data) are the corresponding response outputs.
- Step 4. *Train ROMs for the objectives of interest*: A reduced-order model is used to map the relationship between the training parameters inputs and outputs. We build an ensemble of ROMs, one for each objective of interest, namely the cumulative  $\text{CO}_2$  leakage ( $M_c$ ) and the simulated monitoring data ( $D$ ) at each specified time-step. A fully-connected artificial neural network (ANN) is implemented to build the ROMs.
- Step 5. *Validate the ROMs against the high-fidelity simulations*: Using 10-fold cross-validation, we test the predictions from the ROMs against the HFS results in order to perform hyper-parameter tuning and obtain robust ROMs that can be used for further predictions.

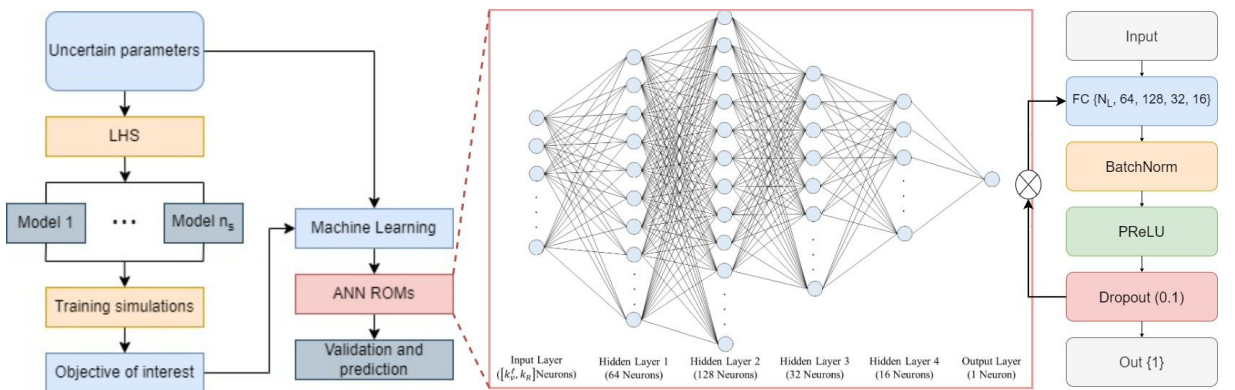


**Figure 1:** Workflow diagram for machine learning-based ROM.

Using the Python TensorFlow/Keras packages [47], we develop a fully-connected ANN architecture to build the ROMs. Each ANN consists of four hidden layers with sizes 64, 128, 32, and 16, respectively, with a total number of parameters equal to 14,705, as shown in Fig.1. A kernel regularizer is applied to each hidden layer using the  $\ell_1$ -norm, and dropout of 10% is used on each hidden layer. The activation function for each layer is the parametric rectified linear unit (PReLU), which learns the negative slope for each batch in each epoch. The Adam optimizer is used with a

mean squared error (MSE) loss function. A total of 500 HFS realizations are obtained and used to train the ANN ROM (more details in Sections 2.4 and 3.1). 400 realizations are used for training and 100 for blind testing. During training, a batch size of 40 is used, and for each batch a random subset of 10% are used as validation. Training is performed on an NVIDIA RTX A6000 GPU in about 2 minutes. The average validation MSE is approximately  $8.5 \times 10^{-4}$  and the correlation coefficient ( $R^2$ ) is approximately 0.98. The truth vs. prediction performance for a set of 500 realizations of uncertain parameters is shown in Fig.2 as a comparison of the accuracy of our ANN ROM and the MARS ROM in Chen et al. [42]. The average prediction time for the ANN ROMs is approximately 0.5ms with an  $R^2$  value of 0.993, showing a significant improvement over the MARS ROMs which require 70.37ms for each prediction and  $R^2 = 0.976$ .

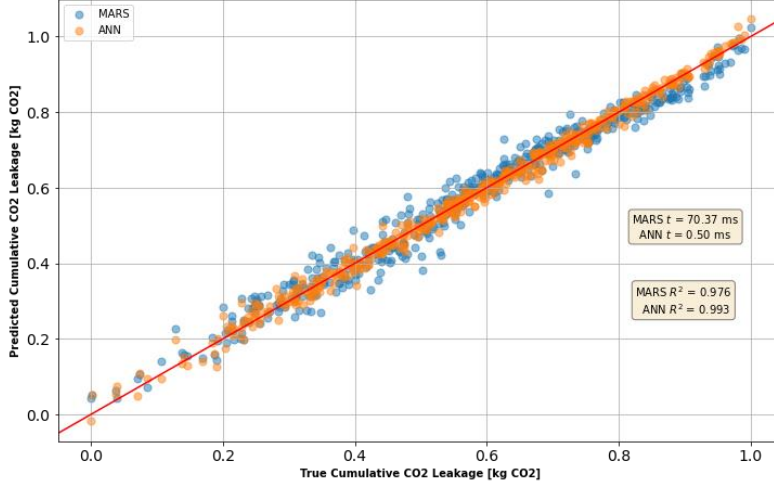


**Figure 2:** Cumulative CO<sub>2</sub> leakage prediction from ANN ROM (orange) and MARS ROM (blue) vs true cumulative CO<sub>2</sub> leakage. The ANN ROM requires an average of 0.50ms per prediction with an  $R^2$  of 0.993, while the MARS ROM require an average of 70.37ms per prediction with an  $R^2$  of 0.976.

### 2.3. Workflow for Optimal Monitoring Design

In this section, we present a filtering and ROM based workflow for optimal monitoring design of GCS. The workflow diagram is shown in Fig. 3. The main steps for the optimal monitoring design workflow are summarized below.

- Step 1. *Develop ROMs for the objective function,  $M_c$ , and predict monitoring data,  $D$ .* A detailed description of the ROM development workflow were presented in the previous section. We build one ROM for each monitoring data point,  $d_i$ , in each data vector  $D^j$ . The vector of predicted monitoring data is denoted as  $O(m) = [O_1(m), O_2(m), \dots, O_{n_d}(m)]^T$ , where  $m$  is the vector of uncertain model input parameters, namely  $k_v^\ell$  and  $k_R$ . The ROMs are used to replace FEHM physics-based simulations and to predict the objectives of interest for a set of new input parameters not in the training data.
- Step 2. *Generate an ensemble of realizations of monitoring data,  $D$ .* Initially,  $l_d$  realizations are sampled from the prior PDF of  $m$ , and are denoted as  $\{\tilde{m}^j\}_{j=1}^{l_d}$ . The corresponding monitoring data,  $\tilde{d}_{obs}^j$ , for each  $\tilde{m}^j$  are given by:

$$\tilde{d}_{obs}^j = O(\tilde{m}^j) + e^j, \quad (4)$$

where  $O(\tilde{m}^j)$  is the ROM prediction for  $n_d$  monitoring data points and  $e^j$  denotes the  $j^{th}$  realization of measurement errors which follow a Gaussian distribution.

- Step 3. *Generate Monte Carlo samples, and calculate prior uncertainty.* A large number (50,000) Monte Carlo samples are generated from the prior distribution of  $m$ , and denotes as  $\{\hat{m}^k\}_{k=1}^{\ell_{MC}}$ . The Monte Carlo samples are used to calculate the prior PDF and the amount of uncertainty in the prior is computed using Eq. (1).



Step 4. *Filter the Monte Carlo samples, and compute expected posterior uncertainty.* Using a filtering-based method [34], also known as rejection sampling, we construct a posterior distribution of  $m$  conditional to each  $\tilde{d}_{obs}^j$ . First, using the Monte Carlo samples,  $\hat{m}^k$ , generated in Step 3, we simulate the corresponding monitoring data  $\hat{d}^k$  with the ROMs generated in Step 1, such that  $\hat{d}^k = O(\hat{m}^k)$ . Here,  $\hat{d}^k$  represents a realization from the distribution of potential monitoring data sets that capture potential CO<sub>2</sub> leakage scenarios given the uncertain input parameters  $k_v^\ell$  and  $k_R$ . The data assimilation error is defined as the maximum absolute error (MAE) as follows:

$$MAE(d_{obs}^j) = \max_{1 \leq i \leq n_d} |\tilde{d}_{obs,i}^j - \hat{d}_i^k|. \quad (5)$$

Given a threshold value  $\tau$ , the  $\hat{m}^k$  sample is accepted as a legitimate realization of the posterior distribution according to the following acceptance probability:

$$P_{acc}(\hat{m}^k) = \begin{cases} 1, & \text{if } MAE < \tau, \\ 0, & \text{otherwise.} \end{cases} \quad (6)$$

The threshold value,  $\tau$ , is chosen based on engineering judgement and takes into consideration the measurement and modeling errors. Therefore,  $\hat{m}^k$  is accepted if it is deemed sufficiently consistent with the true monitoring data realization. Every Monte Carlo sample is evaluated using Eq. (6) and the accepted samples constitute the posterior distribution of  $m$  conditional to the monitoring data realization  $\tilde{d}_{obs}^j$  such that  $\ell_d$  posterior samples of  $m$  are obtained. The expected posterior uncertainty is calculated using Eq. (2).

Step 5. *Calculate the expected amount of uncertainty reduction  $U_R$ .* The expected amount of uncertainty reduction,  $U_R$ , is calculated by comparing the uncertainty in the prior distribution and the expected value of the uncertainty in the posterior distribution using Eq. (3).

Step 6. *Monitoring well placement optimization.* We repeat Steps 2-5 for every possible monitoring well location in the GCS area of review (AOR), conditional to the data for each possible measurement type,  $D^j$ . We calculate the expected amount of uncertainty reduction for each monitoring data type,  $D^j$ , for each possible monitoring well location  $\{x^p\}_{p=1}^{16}$ , and obtain the monitoring design that maximally reduces the uncertainty in cumulative CO<sub>2</sub> leakage (maximally reducing the uncertainty is equivalent to minimizing the negative expected uncertainty reduction), as shown in Eq. (7)

$$x_p^* = \min_{1 \leq p \leq 16} -U_R^{x_p}. \quad (7)$$

This results in an exhaustive search in the subgrid to obtain the optimal well location,  $x_p^*$ , that yields the highest uncertainty reduction, defined by  $U_R^{x_p}$  as follows:

$$U_R^{x_p} = U^{x_p}[P(M_c)] - E_d[U^{x_p}[P(M_c|D^j)]]. \quad (8)$$

With this optimal monitoring design workflow, the expected uncertainty reduction in cumulative CO<sub>2</sub> leakage for each potential monitoring measurement, and each potential monitoring well location are computed, and the optimal monitoring design that reduces the uncertainty in the simulated amount of CO<sub>2</sub> leakage is obtained.

## 2.4. Model Description

We implement the optimal monitoring design workflow on a synthetic GCS model consisting of a heterogeneous storage reservoir, a homogeneous caprock layer and a homogeneous aquifer, as shown in the schematic of the base model in Fig. 4. The storage reservoir itself is a fully-saturated saline aquifer, while the homogeneous aquifer zone above the caprock layer is a potential underground source of drinking water (USDW). The thickness of each of the three layers is 30 m, and the model is 1 km wide in the horizontal dimensions. The depth from ground surface to the top of the model is 1000 m. A CO<sub>2</sub> injection well is placed at the center of the reservoir and multiple potential leakage pathways traverse the caprock, where CO<sub>2</sub> could possibly leak into the potential USDW aquifer. Note that only one possible leakage pathway is shown in Fig. 4, while we have considered several scenarios with multiple potential leakage pathways. The caprock and potential USDW aquifer layers are assumed to have a homogeneous permeability

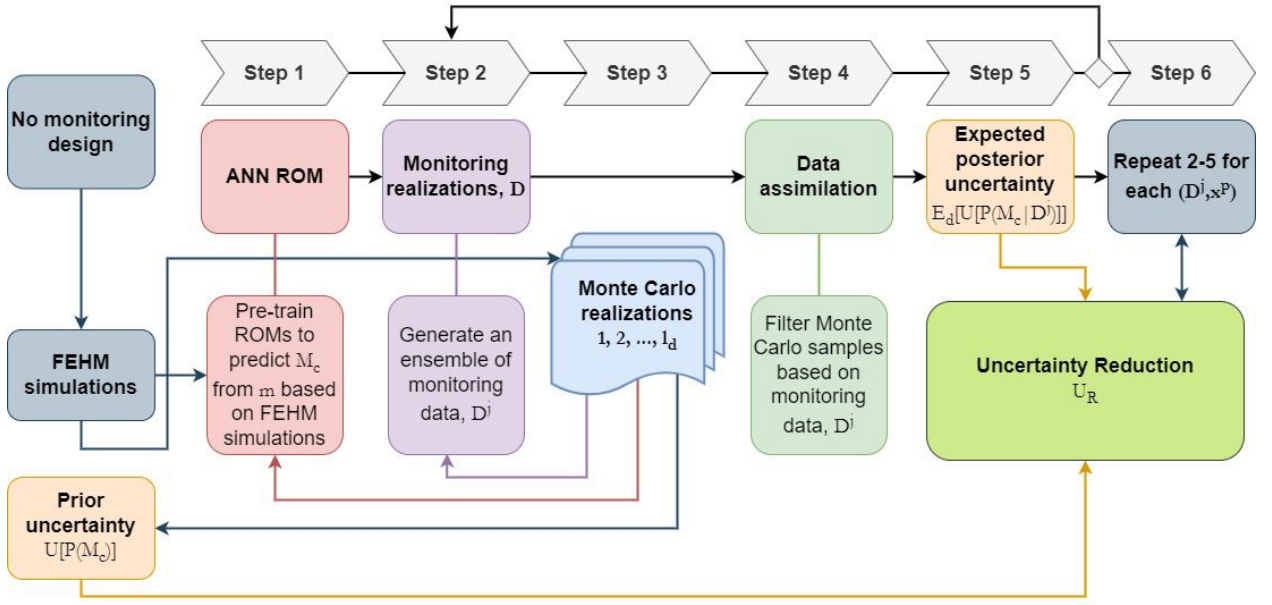


**Figure 3:** Workflow diagram for optimal monitoring design. First, calculate the prior uncertainty with no monitoring design based on Monte Carlo samples. Then use the pre-trained ROMs to predict  $\text{CO}_2$  cumulative leakage using Monte Carlo samples and perform data assimilation of monitoring measurement  $D^j$  for monitoring well placement  $x^p$  to compute expected posterior uncertainty. The uncertainty reduction for case  $(D^j, x^p)$  is given by  $U^{x_p}[P(M_c)] - E_d[U^{x_p}[P(M_c|D^j)]]$ , and we repeat for each possible  $D^j$  and  $x^p$ .

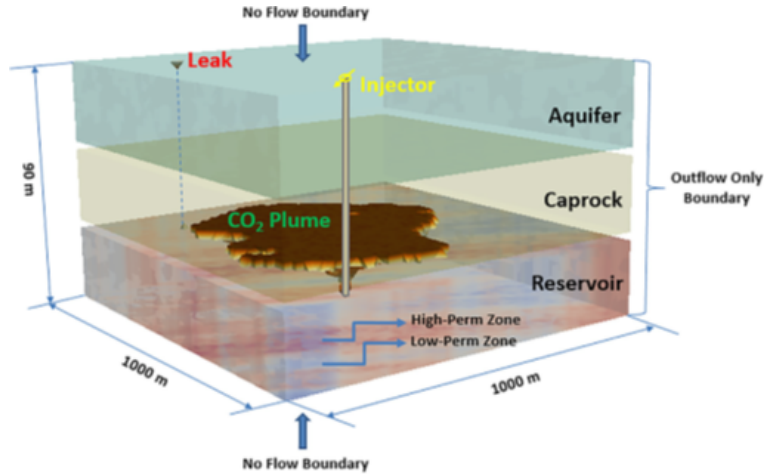


**Figure 4:** Schematic of the base model, in which a storage reservoir and potential USDW aquifer are separated by a caprock. At the center is a  $\text{CO}_2$  injection well. The vertical axis is exaggerated 7 times.

distribution equal to  $1 \times 10^{-19} \text{ m}^2$  and  $1 \times 10^{-13} \text{ m}^2$ , respectively. The storage reservoir has a heterogeneous permeability distribution, as shown in Fig. 5. The base model is generated using a spherical variogram model [48, 49] with major and minor correlation lengths of 680 m and 280 m, respectively, with a major direction of  $45^\circ$  from the positive  $x$ -axis.

The mean of the permeability field is  $1 \times 10^{-13} \text{ m}^2$ . For each realization, we assume that the reservoir permeability is uncertain, and to honor this uncertainty we use a permeability multiplier,  $k_R$ , to multiply the aforementioned base permeability distribution. The lower and upper bounds for the multiplier  $k_R$  and the potential leaky pathways  $k_v^\ell$  are shown in Table 1.

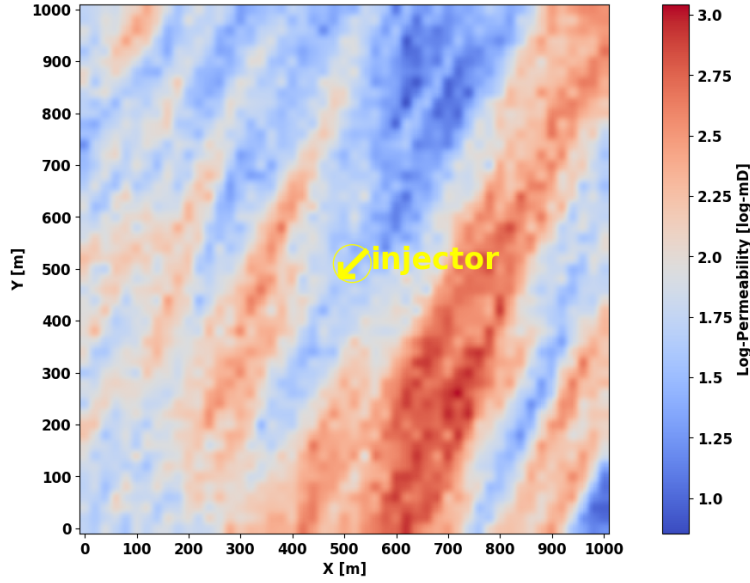


**Figure 5:** Log-permeability distribution of the base model. The darkest blue color corresponds to the lowest permeability, while the darkest red color corresponds to the highest. The yellow circle with an arrow indicates the CO<sub>2</sub> injection well.

**Table 1**

Uncertain parameters and their lower and upper bounds.

Uncertain parameters	Symbol	Lower bound	Upper bound	Unit
Reservoir permeability multiplier	$k_R$	0.5	2	—
Permeability of leaky pathway(s)	$k_v^\ell$	-19 0.001	-14 10	$\log_{10} [m^2]$ $mD$

A numerical mesh for the reservoir simulation is made using the grid generation toolkit *LaGriT* [50]. The numerical mesh has 51 grid nodes in both the  $x$ - and  $y$ -directions, and 31 grid nodes in the  $z$ -direction. The distance between each grid node in the  $x$ - and  $y$ -directions is 20 m, and in the  $z$ -direction it is 3 m. The total number of grid nodes used in the simulation is 80,631, with 26,010 grid nodes in the reservoir and caprock, respectively, and 28,611 grid nodes in the potential USDW aquifer. FEHM is used for 3D multi-phase flow simulations [46]. The boundary conditions of the reservoir are defined as Dirichlet boundaries, allowing CO<sub>2</sub> to flow out but not in, and water pressure above hydrostatic. The top and bottom boundary conditions of the simulation model are no-flow boundaries. The thermal conditions of the model are initialized using a geothermal gradient of 0.03°C/m with a temperature of 20°C at the top. Pressure gradients are initialized at  $9.81 \times 10^{-3}$  MPa/m with an additional overburden pressure of 0.2 MPa along the top such that the average reservoir pressure in the first layer is approximately 10 MPa. CO<sub>2</sub> is constantly injected in a five-year period, monitored monthly, with a constant injection rate of 0.1 million metric tons/year.

### 3. Results

In this section, we apply our optimal monitoring design workflow using the ANN ROMs and filter-based uncertainty quantification approach to obtain the optimal monitoring well placement and monitoring measurement data type for two synthetic GCS examples.

#### 3.1. Workflow Validation

We validate the workflow for optimal GCS monitoring design using a simple example. Fig. 5 shows the log-permeability distribution for the base model with a CO<sub>2</sub> injection well at the center, noted with a yellow circle and arrow. All the monitoring data are collected in the potential USDW aquifer zone, similar to monitoring at the above



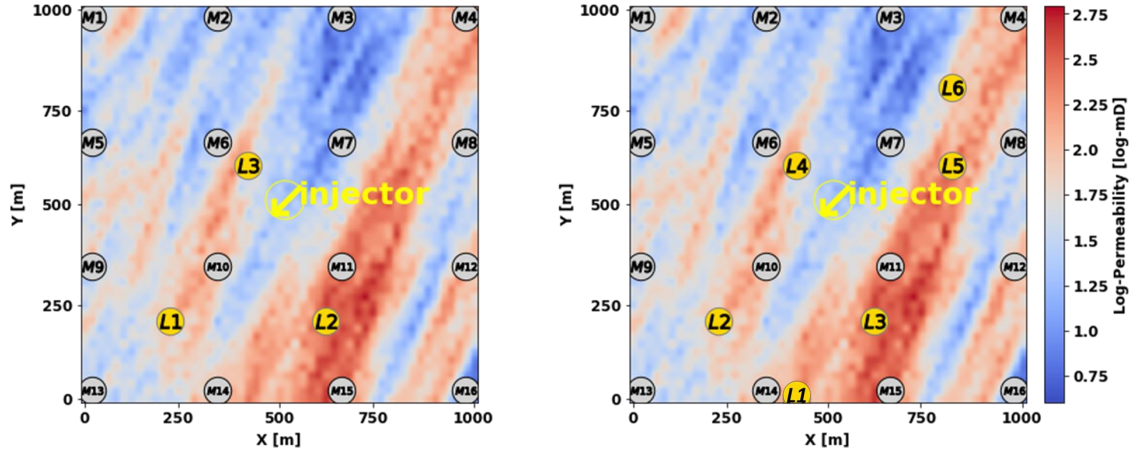


**Figure 6:** Log-permeability distribution of the base model for Case 1 (left) with 3 potential leaky pathways, and Case 2 (right) with 6 potential leaky pathways. The dark yellow circles labeled  $L_i$  represent the leakage pathways, light gray circles labels  $M_i$  are the possible monitoring well locations, and the yellow circle with an arrow is the  $\text{CO}_2$  injection well.

zone monitoring interval (AZMI) in the work of Sun et al. [21]. The monitoring frequency is once per month for the duration of 5 years injection, resulting in 60 monitoring data points. The objective function,  $M_c$ , is the cumulative  $\text{CO}_2$  leakage through legacy wells at the end of 5 years. In the model, we set up three material zones corresponding to the three adjacent formations, namely the storage reservoir, caprock, and potential USDW aquifer. The cumulative  $\text{CO}_2$  saturation in each zone is output from the Finite Element Heat and Mass Transfer (FEHM) [46] simulation results, and the cumulative leakage is computed by summing the  $\text{CO}_2$  mass in the potential USDW aquifer and caprock layers. We coarsen the simulation grid into a  $4 \times 4$  subgrid, meaning there are 16 possible monitoring well locations. Our approach for monitoring design involves quantifying the uncertainty reduction by monitoring pressure,  $\text{CO}_2$  saturation, and/or temperature at each potential monitoring well location.

The data assimilation error tolerance,  $\tau$  from Eq. (6), for pressure is set equal to 0.002 MPa, while for  $\text{CO}_2$  saturation it is 0.05, and for temperature it is  $0.002^\circ\text{C}$ . Note that the choice of  $\tau$  is site specific and is based on engineering judgement that takes into consideration the measurement and modeling error. In this case, the values of  $\tau$  are determined empirically as 1% of the variance in the observed measurements.

We consider two case studies: (1) GCS project with 3 potential leakage pathways (i.e., legacy wells), and (2) GCS project with 6 potential leakage pathways. The uncertain parameters are the permeability multiplier,  $k_R$  for the storage reservoir, and the  $\ell$  permeability values for the  $\ell$  potential leakage pathways, where  $\ell = 3$  and  $\ell = 6$ , respectively. The total number of uncertain parameters,  $u^\ell$  are 4 and 7, respectively. The lower and upper bounds for the uncertain parameters are shown in Table 1. For each case study, we run 500 training simulations generated by LHS with  $u^\ell$  uncertain parameters. Each HFS requires approximately 22 minutes. We perform parallelization on an 8-node cluster, and the total simulation time is approximately 23 hours to finish all 500 training realizations. Fig. 6 shows the base model for Case 1 and Case 2, respectively.

We choose one simulation from the 500 training realizations in Case 1 to show when  $\text{CO}_2$  leakage occurs. The values of the different parameters for the chosen model are shown in Table 2. The cumulative  $\text{CO}_2$  leakage over the GCS project time is shown in Fig. 7. It is observed that  $\text{CO}_2$  leakage occurs after about 210 days of injection. We observe that  $\text{CO}_2$  is leaking through the potential pathway  $L_3$ , which is 141.4 m away from the injector, while no leakage occurs at potential pathways  $L_1$  and  $L_2$  after 5 years of injection. For this specific example, it is important to note that the effective well permeability of  $L_3$ ,  $k_v^3$ , is higher than that of  $L_1$  and  $L_2$ .

**Table 2**

The parameters for one chosen model from the 500 training realizations in Case 1.

Parameters	Value	Unit
CO <sub>2</sub> injection rate	3.17	kg/s
Thickness of caprock layer	30	m
Permeability of 1 <sup>st</sup> potential leakage pathway	$2.19 \times 10^{-17}$	$m^2$
Permeability of 2 <sup>nd</sup> potential leakage pathway	$3.37 \times 10^{-17}$	$m^2$
Permeability of 3 <sup>rd</sup> potential leakage pathway	$2.97 \times 10^{-16}$	$m^2$
Distance between injector and 1 <sup>st</sup> potential leakage pathway	424.3	m
Distance between injector and 2 <sup>nd</sup> potential leakage pathway	360.6	m
Distance between injector and 3 <sup>rd</sup> potential leakage pathway	141.4	m
Permeability for potential USDW aquifer layer	$1 \times 10^{-13}$	$m^2$
Permeability for caprock layer	$1 \times 10^{-19}$	$m^2$
Reservoir permeability multiplier	1.88	—

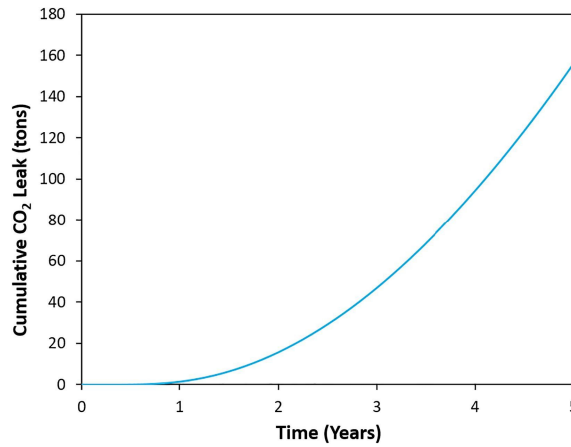


**Figure 7:** Cumulative CO<sub>2</sub> leakage over time computed for one chosen training realization in Case 1.

For each case, the 500 training realizations are used to train ROMs for the monitoring data and cumulative CO<sub>2</sub> leakage using the ANN architecture in Fig 1. Fig. 2 shows the quality of the ROMs tested by 10-fold cross-validation [51, 52]. The MSE and  $R^2$  are  $8.5 \times 10^{-4}$  and 0.98, respectively. This proves that the fidelity of ROMs to the numerical simulations is high at the advantage of a much lower computational cost.

With the proposed workflow, the expected uncertainty reduction of the cumulative CO<sub>2</sub> leakage is computed for each of the 16 possible monitoring well locations, for each monitoring measurement type. For each data set, 200 possible realizations of monitoring data are generated following Step 2 in Section 2.4. To obtain the expected uncertainty reduction using Eq. (3), the prior uncertainty  $U[P(M_c)]$  and posterior uncertainty  $U[P(M_c|D^j)]$  corresponding to each possible monitoring data realization  $D^j$  for each possible well location  $x^p$  should be computed. Higher uncertainty reduction of the objective function indicates greater VOI in the monitoring data obtained from the optimal well location and monitoring measurement type. Through these examples, we can see that our proposed workflow is effectively used to determine optimal CO<sub>2</sub> monitoring design from a set of alternative monitoring designs.

We observe that monitoring for pressure provides the highest uncertainty reduction in general, followed by CO<sub>2</sub> saturation and lastly pressure, as shown in Figures 8 and 9. The spatial distribution of uncertainty reduction in CO<sub>2</sub> leakage is shown in Fig. 8 for every possible well location  $x^p$  in the  $4 \times 4$  subgrid, and point-wise comparison of the uncertainty reduction at each monitoring well location for each measurement type is shown in Fig. 9. One can observe that placing a monitoring well at location 6 (i.e.,  $M6$ ) and assimilation the pressure measurements provides the highest uncertainty reduction possible in the monitoring design for both Case 1 and Case 2. For Case 1, the optimal monitoring design given by (*pressure*, 6) yields an uncertainty reduction in the cumulative leakage of CO<sub>2</sub> of approximately  $29.42 \times 10^3$  metric tons (29.24 kt), approximately a 73% reduction. Meanwhile, the optimal design

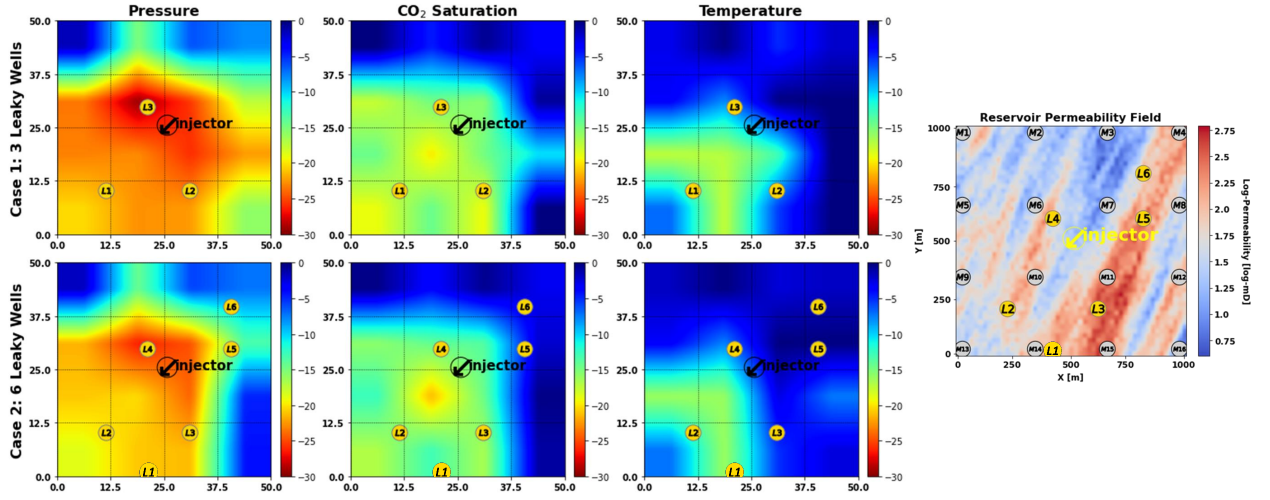


**Figure 8:** Left: Plan view (top of the aquifer layer) of the uncertainty reduction obtained by all possible monitoring well locations. Top row represents Case 1 with 3 leakage pathways, and the bottom row represents Case 2 with 6 leakage pathways. Each column represents monitoring data for pressure, CO<sub>2</sub> saturation, and temperature, respectively. Right: Plan view of the reservoir permeability field with possible leakage pathways (yellow) and all possible monitoring well locations (gray).

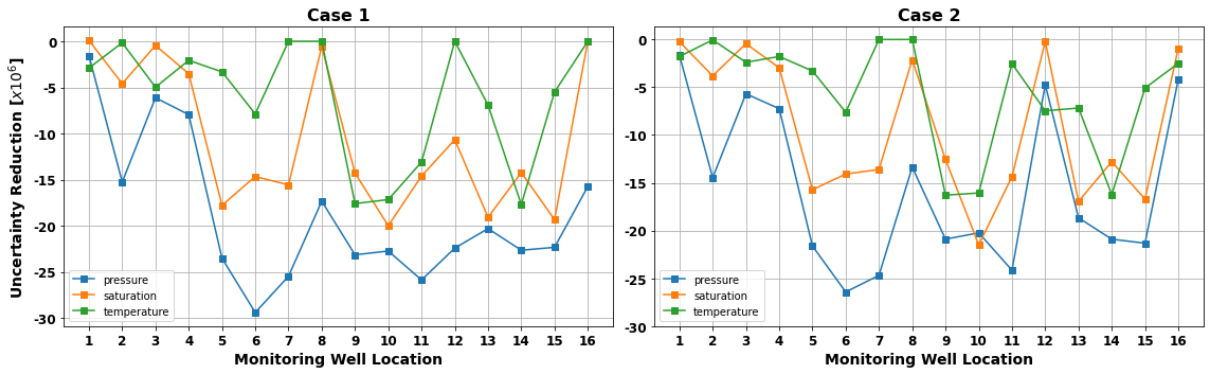


**Figure 9:** Point-wise calculated uncertainty reduction at each possible monitoring well location for each measurement type. Case 1 is shown on the left, and Case 2 on the right.

for CO<sub>2</sub> saturation and temperature monitoring yield an uncertainty reduction of approximately 19.34 kt and 17.71 kt, respectively. Similarly, for Case 2, the optimal monitoring design given by (*pressure*, 6) yields an uncertainty reduction of 26.29 kt of cumulative CO<sub>2</sub> leakage, a 62% reduction, while the optimal design for CO<sub>2</sub> saturation and temperature monitoring yield an uncertainty reduction of approximately 16.94 kt and 16.29 kt, respectively.

The histograms for the prior and posterior distributions of the objective function obtained from the data realizations 1 and 100 for Case 1 and 2, respectively, are shown in Fig. 10. The prior distribution is generated using LHS from the set of uncertain input parameters,  $k_V^L$  and  $k_R$ , with a uniform distribution and calculating the cumulative CO<sub>2</sub> leakage using the ROMs. The posterior distribution for two random realizations, namely realization 1 and 100, are shown.

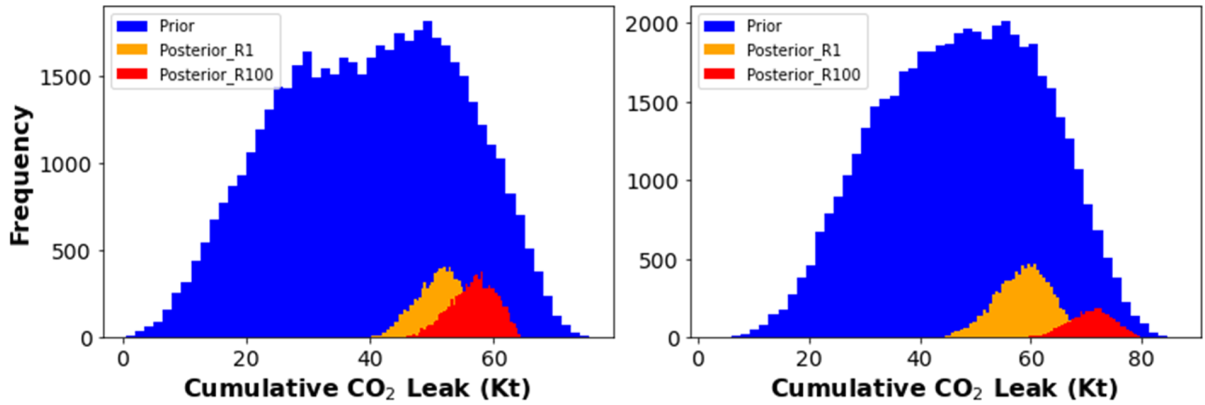


**Figure 10:** Histograms for the prior (blue) and posterior distributions obtained at the optimal monitoring design from the data realizations 1 (orange) and 100 (red) for Case 1 (left) and Case 2 (right), respectively.

These two are selected given that they have a relatively high amount of cumulative CO<sub>2</sub> leakage. Recall that the total uncertainty reduction,  $U_R$  is given by the difference between the expected posterior uncertainty (the expected value of the ensemble of realizations) and the prior uncertainty distribution. Figure 10 shows the prior and posterior distributions on the same figure by using the same number of bins despite having different bin widths to elucidate the reduction in uncertainty after data assimilation. The variances of the posterior distributions calculated show significant reduction in uncertainty of cumulative CO<sub>2</sub> leakage compared to the priors. The optimal monitoring design (*pressure*, 6) yields a reduction in cumulative CO<sub>2</sub> leakage uncertainty of approximately 29.24 kt (73%) and 26.29 kt (62%) for Case 1 and Case 2, respectively.

### 3.2. Discussion

GCS monitoring operations require detailed data processing and interpretation in order to accurately quantify and potentially minimize leakage risks. Associated costs of performing monitoring operations requires evaluating the potential value of monitoring measurement type, and optimal monitoring well location, before the actual monitoring strategy takes place in the field. The workflow proposed is used to select an optimal monitoring design that is robust under multiple potential leakage scenarios. Previous efforts show the importance of characterizing the geologic uncertainty in GCS projects [20, 31, 41], selecting the optimal measurement type [37, 38], or selecting the optimal monitoring well location [17, 21]. Our work builds upon the work of Chen et al. [42] to provide a workflow to unify these three concepts under a single optimal monitoring design framework.

The difference in uncertainty reduction between Case 1 and Case 2, despite the fact that we have more leakage pathways, is attributed to the fact that the main source of uncertainty is the geologic parameters, namely  $k_v^\ell$  and  $k_R$ , rather than the number of leakage pathways. These parameters ultimately control the leaking of CO<sub>2</sub>, and can range between very small ( $\sim 0.001mD$ ) to medium ( $\sim 10mD$ ). Thus, the cumulative CO<sub>2</sub> leakage in our specific cases correlates with the permeability of the leakage pathways,  $k_v^\ell$ , and the reservoir permeability multiplier,  $k_R$ , more strongly than with having more or less number leakage pathways. In other cases, one might find that effective wellbore permeability for legacy wells is more strongly correlated to cumulative CO<sub>2</sub> leakage. For instance, wells 6-7 and 10-11 lie closest to the injection well at approximately 176.8 m, yet well 6 yields the highest uncertainty reduction since it is closest to a high permeability streak, similar to well 11. On the other hand, well 7 lie on low permeability streaks, making the plumes travel relatively slower. Therefore, the distance of the potential monitoring location from injector and leakage pathways is important, but mostly controlled by the permeability heterogeneity in the reservoir. The legacy wells,  $L_1 - L_6$  are preferentially drilled in high permeability zones of the reservoir, but the permeability distribution and transitions between the injector well and legacy wells are critical to the uncertainty in leakage. Therefore, these relationships play a crucial role in optimal monitoring locations.

Furthermore, it is evident that monitoring for pressure data yields the highest uncertainty reduction out of the three possible measurement types. This is due to the fact that the pressure fronts travel the fastest along a given subsurface formation, followed by saturation plumes and temperature plumes, in that order [53]. Temperature plumes tend to

travel the least, given the thermal equilibrium of deep underground formations and the gradual enthalpy change in the reaction of  $\text{CO}_2$  in saline aquifers [54]. In some monitoring locations, such as wells 7 and 8, monitoring for temperature provides little to no uncertainty reduction whatsoever, while pressure monitoring yields about 17-25 kt uncertainty reduction in the cumulative  $\text{CO}_2$  leakage. The total uncertainty reduction given by the sum of all three measurements correlated primarily with the pressure monitoring data, and assimilating multiple measurements types simultaneously does not necessarily add linearly, and tends to be dominated by a single measurement. Refer to Chen et al. [42] for more information on assimilating multiple measurement types simultaneously.

It is also important to note that the monitoring wells are only drilled through the potential USDW aquifer layer, and not the caprock and reservoir, thus only collecting monitoring measurements at the potential USDW aquifer zone. This is way, despite  $x^6$  being further away from the injector than the closest leakage pathway ( $L_3$  in Case 1 and  $L_4$  in Case 2), it still provides the most information about  $\text{CO}_2$  leakage into the potential USDW aquifer zone. Also, recall the potential USDW aquifer is geologically homogeneous, and the pressure,  $\text{CO}_2$  saturation, and temperature response does not necessarily exactly correlate with the reservoir response.

There are several limitations in our proposed method. Firstly, regarding the monitoring well location grid, location  $x^6$  yields the highest uncertainty reduction when using pressure measurements for both Case 1 and Case 2. However, the 16 possible monitoring well locations exist on a coarse  $4 \times 4$  subgrid. Monitoring location  $x^6$  is closest to the injection well and a leakage pathway in both Case 1 and Case 2, and therefore provides the best uncertainty reduction. However, if a finer monitoring well location grid were used, i.e.,  $16 \times 16$  or  $32 \times 32$  (which is still coarser than the simulation grid at  $51 \times 51$ ), a location between the injector well and  $L_3$  in Case 1 and  $L_4$  in Case 2 would most likely yield the best uncertainty reduction. This is due to the fact that a monitoring well in that location would be able to detect the  $\text{CO}_2$  plume before it even reaches and leakage pathways, and would still be in the region of high permeability in the reservoir, thus yielding the best uncertainty reduction in cumulative  $\text{CO}_2$  leakage. Future work would include conducting case studies with finer monitoring well location grids to obtain uncertainty reduction values at more refined locations.

A second limitation is that due to the fact that we are using a coarse monitoring well location grid, several locations such as  $M_{1-4}$ ,  $M_8$ ,  $M_{12}$ , and  $M_{14-15}$  yield little to no uncertainty reduction. We stipulate that this occurs because the  $\text{CO}_2$  plume reaches the leakage pathways before it reaches these monitoring wells, and therefore provide little information to the data assimilation to reduce the uncertainty in leakage. This also leads to the idea that most of the  $\text{CO}_2$  leakage is occurring in the pathways closest to the injection well, and thus the closer monitoring locations provide a better uncertainty reduction than those in the boundaries or further away. This relates to the fact that despite Case 2 having more leakage pathways, the uncertainty reduction in kt of  $\text{CO}_2$  is not much different from that of Case 1.

Other limitations include the assumption that we can model the storage reservoir, caprock, and potential USDW aquifer using a structured grid, and that monitoring data is collected at a regular schedule and assumed to be exactly true. Furthermore, the ANN ROM is trained on a single synthetic geologic model with variable uncertain parameters, and would require re-training or modifying the architecture in order to implement in a different geologic model or a real-world field case.

Even though the examples used in our study to demonstrate how monitoring data from a potential USDW aquifer can be used, the proposed workflow can be extended and applied to monitoring data collected at any location (e.g., monitoring from storage reservoir and/or AZMI) and time within the GCS project. The potential value of such monitoring data can be evaluated by the presented workflow. Furthermore, placing several monitoring wells paired with one injector can provide a slight advantage compared to a single injector-monitor pair, but is impractical in field applications due to high cost in drilling monitoring wells. Moreover, using several monitoring measurement types simultaneously provides little to no advantage compared to pressure monitoring.

## 4. Conclusions

We propose a workflow based on a machine learning reduced-order modeling technique and uncertainty quantification method within an optimization loop for geologic  $\text{CO}_2$  sequestration monitoring design. We use the uncertainty reduction in cumulative  $\text{CO}_2$  leakage as the quantity of interest to measure the potential value of monitoring measurement data. The optimal monitoring design yields an uncertainty reduction of approximately 29.94 kt (73%) and 26.29 kt (62%) in  $\text{CO}_2$  leakage for Case 1 and Case 2, respectively. The following conclusions have been drawn from this research:



1. The proposed workflow can generate reasonable values of uncertainty reduction in different risk quantities at CO<sub>2</sub> storage site, including cumulative CO<sub>2</sub> leakage by utilizing different monitoring designs and has been demonstrated using a synthetic GCS project. The optimal monitoring design is obtained by assimilating pressure data at location 6 for a monitoring well.
2. The effect of different types of measurements (pressure, CO<sub>2</sub> saturation, and temperature) and the effect of monitoring well location on the choice of monitoring design is investigated. It is observed that pressure data has more value of information compared to CO<sub>2</sub> saturation, while temperature has the least value of information, though still valuable in terms of uncertainty reduction compared to no monitoring strategy.
3. Well placement optimization is important to maximize the value of information for the monitoring design. Typical operations include pairs of one monitoring well for each injection well, partly due to the cost of drilling and data acquisition. Determination of the best location provides significant benefits in reducing the uncertainty of cumulative CO<sub>2</sub> leakage and ensure an efficient risk management in the life-cycle of a GCS project.
4. The incremental reduction in uncertainty in the cumulative CO<sub>2</sub> leakage may not increase proportional to the distance from the injection well, and is a strong function of the reservoir permeability heterogeneity. Thus, an optimal monitoring well placement and measurement type is important to minimize present and future potential risks.
5. The subgrid for the possible monitoring well locations will have a major impact in the optimal monitoring design. The uncertainty reduction obtained at the monitoring locations will depend on the geologic heterogeneity, which affects the CO<sub>2</sub> plume movement in the subsurface. However, with proper knowledge of the geologic setting and a finer monitoring location subgrid, one can further optimize the monitoring design to further reduce the uncertainty in cumulative CO<sub>2</sub> leakage.

Future research in this topic includes investigating the effect of different monitoring measurement types, such as seismic sensing, or a combination of the available measurements. Another possible direction is to compare different methods for reduced-order modeling and cumulative leakage quantification, including analytical-based methods or more advanced machine learning-based techniques. Furthermore, multi-scale or local grid refinement could be applied to optimize the monitoring well placement and help improve the reduction in uncertainty for CO<sub>2</sub> leakage risks. Moreover, a global optimization strategy, such as genetic algorithm or simulated annealing, can provide more computationally efficient results for finer subgrids. Other alternatives could include incorporating other data assimilation techniques such as EnKF or ES-MDA, or performing spatial data assimilation rather than assimilating point-wise measurements. Including other risks such as geomechanical failure can help characterize a GCS site and provide a more in-depth risk management program.

## CRediT authorship contribution statement

**Misael M. Morales:** Conceptualization, Methodology, Software, Writing - Original draft. **Mohamed Mehana:** Conceptualization, Supervision, Writing - review & editing. **Carlos Torres-Verdín:** Writing - review & editing. **Michael J. Pyrcz:** Writing - review & editing. **Bailian Chen:** Conceptualization, Software, Funding acquisition, Supervision, Writing - review & editing.

## References

- [1] Bert Metz. Carbon dioxide capture and storage: special report of the intergovernmental panel on climate change, 2005.
- [2] Mai Bui, Claire S. Adjiman, André Bardow, Edward J. Anthony, Andy Boston, Solomon Brown, Paul S. Fennell, Sabine Fuss, Amparo Galindo, Leigh A. Hackett, Jason P. Hallett, Howard J. Herzog, George Jackson, Jasmin Kemper, Samuel Krevor, Geoffrey C. Maitland, Michael Matuszewski, Ian S. Metcalfe, Camille Petit, Graeme Puxty, Jeffrey Reimer, David M. Reiner, Edward S. Rubin, Stuart A. Scott, Nilay Shah, Berend Smit, J. P. Martin Trusler, Paul Webley, Jennifer Wilcox, and Niall Mac Dowell. Carbon capture and storage (ccs): the way forward. *Energy Environ. Sci.*, 11:1062–1176, 2018. doi: 10.1039/C7EE02342A. URL <http://dx.doi.org/10.1039/C7EE02342A>.
- [3] United nations. Agreement, p. *United Nations Treaty Collect*, pages 1–27, 2015.
- [4] Zhenxue Dai, Hari Viswanathan, Richard Middleton, Feng Pan, William Ampomah, Changbing Yang, Wei Jia, Ting Xiao, Si Yong Lee, Brian McPherson, Robert Balch, Reid Grigg, and Mark White. Co2 accounting and risk analysis for co2 sequestration at enhanced oil recovery sites. *Environmental Science and Technology*, 50(14):7546–7554, 7 2016. ISSN 15205851. doi: 10.1021/acs.est.6b01744.
- [5] D.R. Harp, R. Pawar, J.W. Carey, and C.W. Gable. Reduced order models of transient co2 and brine leakage along abandoned wellbores from geologic carbon sequestration reservoirs. *International Journal of Greenhouse Gas Control*, 45:150–162, 2 2016. ISSN 1750-5836. doi: 10.1016/j.ijggc.2015.12.001. cited By 38.

- [6] J.M. Nordbotten, B. Flemisch, S.E. Gasda, H.M. Nilsen, Y. Fan, G.E. Pickup, B. Wiese, M.A. Celia, H.K. Dahle, G.T. Eigestad, and K. Pruess. Uncertainties in practical simulation of co<sub>2</sub> storage. *International Journal of Greenhouse Gas Control*, 9:234–242, 2012. doi: 10.1016/j.ijggc.2012.03.007. cited By 78.
- [7] S.M. Benson and L. Myer. 2003.
- [8] J. Condor, D. Unatrakarn, M. Wilson, and K. Asghari. A comparative analysis of risk assessment methodologies for the geologic storage of carbon dioxide. volume 4, pages 4036–4043, 2011. doi: 10.1016/j.egypro.2011.02.345.
- [9] J.-P. Nicot, C.M. Oldenburg, J.E. Houseworth, and J.-W. Choi. Analysis of potential leakage pathways at the cranfield, ms, u.s.a., co<sub>2</sub> sequestration site. *International Journal of Greenhouse Gas Control*, 18:388–400, 2013. doi: 10.1016/j.ijggc.2012.10.011. cited By 38.
- [10] R.A. Chadwick, R. Arts, and O. Eiken. 4d seismic quantification of a growing co<sub>2</sub> plume at sleipner, north sea. *Petroleum Geology Conference Proceedings*, 6(0):1385–1399, 2005. doi: 10.1144/0061385. cited By 188.
- [11] R.J. Pawar, G.S. Bromhal, S. Chu, R.M. Dillmore, C.M. Oldenburg, P.H. Stauffer, Y. Zhang, and G.D. Guthrie. The national risk assessment partnership’s integrated assessment model for carbon storage: A tool to support decision making amidst uncertainty. *International Journal of Greenhouse Gas Control*, 52:175–189, 2016. doi: 10.1016/j.ijggc.2016.06.015. cited By 59.
- [12] Y.-M. Yang, M.J. Small, E.O. Ogretim, D.D. Gray, A.W. Wells, G.S. Bromhal, and B.R. Strazisar. A bayesian belief network (bbn) for combining evidence from multiple co<sub>2</sub> leak detection technologies. *Greenhouse Gases: Science and Technology*, 2(3):185–199, 2012. doi: 10.1002/ghg.1284.
- [13] Z. Dai, E. Keating, D. Bacon, H. Viswanathan, P. Stauffer, A. Jordan, and R. Pawar. Probabilistic evaluation of shallow groundwater resources at a hypothetical carbon sequestration site. *Scientific Reports*, 4, 2014. doi: 10.1038/srep04006. cited By 1.
- [14] D. Grana, S. Verma, J. Pafeng, X. Lang, H. Sharma, W. Wu, F. McLaughlin, E. Campbell, K. Ng, V. Alvarado, S. Mallick, and J. Kaszuba. A rock physics and seismic reservoir characterization study of the rock springs uplift, a carbon dioxide sequestration site in southwestern wyoming. *International Journal of Greenhouse Gas Control*, 63:296–309, 2017. doi: 10.1016/j.ijggc.2017.06.004. cited By 23.
- [15] E. Keating, Z. Dai, D. Dempsey, and R. Pawar. Effective detection of co<sub>2</sub> leakage: A comparison of groundwater sampling and pressure monitoring. volume 63, pages 4163–4171, 2014. doi: 10.1016/j.egypro.2014.11.448.
- [16] Z. Wang and M.J. Small. A bayesian approach to co<sub>2</sub> leakage detection at saline sequestration sites using pressure measurements. *International Journal of Greenhouse Gas Control*, 30:188–196, 2014. doi: 10.1016/j.ijggc.2014.09.011.
- [17] Wenye Sun and Louis J. Durlofsky. Data-space approaches for uncertainty quantification of co<sub>2</sub> plume location in geological carbon storage. *Advances in Water Resources*, 123:234–255, 1 2019. ISSN 03091708. doi: 10.1016/j.advwatres.2018.10.028. cited By 23.
- [18] Zhiwei Ma, Yong Do Kim, Oleg Volkov, and Louis J. Durlofsky. Optimization of subsurface flow operations using a dynamic proxy strategy. *Mathematical Geosciences*, 54:1261–1287, 11 2022. ISSN 18748953. doi: 10.1007/S11004-022-10020-2/FIGURES/16.
- [19] J.J. Butler Jr., C.D. McElwee, and G.C. Bohling. Pumping tests in networks of multilevel sampling wells: Motivation and methodology. *Water Resources Research*, 35(11):3553 – 3560, 1999. doi: 10.1029/1999WR900231. Cited by: 92; All Open Access, Bronze Open Access, Green Open Access.
- [20] Bailian Chen, Dylan R. Harp, Zhiming Lu, and Rajesh J. Pawar. Reducing uncertainty in geologic co<sub>2</sub> sequestration risk assessment by assimilating monitoring data. *International Journal of Greenhouse Gas Control*, 94, 3 2020. ISSN 17505836. doi: 10.1016/j.ijggc.2019.102926.
- [21] Alexander Y. Sun, Jean Philippe Nicot, and Xiaodong Zhang. Optimal design of pressure-based, leakage detection monitoring networks for geologic carbon sequestration repositories. *International Journal of Greenhouse Gas Control*, 19:251–261, 2013. ISSN 17505836. doi: 10.1016/j.ijggc.2013.09.005.
- [22] Javier E. Santos, Bernard Chang, Alex Gigliotti, Eric Guiltinan, Mohamed Mehana, Arvind Mohan, James McClure, Qinxun Kang, Hari Viswanathan, Nicholas Lubbers, Masa Prodanovic, and Michael Pyrcz. Learning from a big dataset of digital rock simulations. In *AGU Fall Meeting Abstracts*, volume 2021, pages H250–1207, December 2021.
- [23] E. Laloy, R. Hérault, D. Jacques, and N. Linde. Training-image based geostatistical inversion using a spatial generative adversarial neural network. *Water Resources Research*, 54(1):381–406, 2018. doi: 10.1002/2017WR022148. cited By 206.
- [24] Y. Liu, W. Sun, and L.J. Durlofsky. A deep-learning-based geological parameterization for history matching complex models. *Mathematical Geosciences*, 51(6):725–766, 2019. doi: 10.1007/s11004-019-09794-9. cited By 66.
- [25] B. Chen, J. He, X. Wen, W. Chen, and A. Reynolds. Pilot design analysis using proxies and markov chain monte carlo method. 2016. doi: 10.3997/2214-4609.201601821.
- [26] Z. Guo and A.C. Reynolds. Robust life-cycle production optimization with a support-vector-regression proxy. *SPE Journal*, 23(6):2409–2427, 2018. doi: 10.2118/191378-PA. cited By 88.
- [27] Gege Wen, Zongyi Li, Qirui Long, Kamyar Azizzadenesheli, Anima Anandkumar, and Sally M. Benson. Real-time high-resolution co<sub>2</sub> geological storage prediction using nested fourier neural operators. *Energy & Environmental Science*, 2023. ISSN 1754-5692. doi: 10.1039/d2ee04204e.
- [28] Eduardo Maldonado-Cruz and Michael J. Pyrcz. Fast evaluation of pressure and saturation predictions with a deep learning surrogate flow model. *Journal of Petroleum Science and Engineering*, 212:110244, 5 2022. ISSN 0920-4105. doi: 10.1016/J.PETROL.2022.110244.
- [29] N. Wang, H. Chang, and D. Zhang. Efficient uncertainty quantification for dynamic subsurface flow with surrogate by theory-guided neural network. *Computer Methods in Applied Mechanics and Engineering*, 373, 2021. doi: 10.1016/j.cma.2020.113492. cited By 33.
- [30] B. Chen, J. He, X.-H. Wen, W. Chen, and A.C. Reynolds. Uncertainty quantification and value of information assessment using proxies and markov chain monte carlo method for a pilot project. *Journal of Petroleum Science and Engineering*, 157:328–339, 2017. doi: 10.1016/j.petrol.2017.07.039.
- [31] W. Jia, B. McPherson, F. Pan, Z. Dai, and T. Xiao. Uncertainty quantification of co<sub>2</sub> storage using bayesian model averaging and polynomial chaos expansion. *International Journal of Greenhouse Gas Control*, 71:104–115, 2018. doi: 10.1016/j.ijggc.2018.02.015. cited By 23.
- [32] A.A. Emerick and A.C. Reynolds. Combining the ensemble kalman filter with markov chain monte carlo for improved history matching and uncertainty characterization. *SPE Journal*, 17(2):418–440, 2012. doi: 10.2118/141336-PA.

- [33] Y. Chen and D.S. Oliver. Ensemble randomized maximum likelihood method as an iterative ensemble smoother. *Mathematical Geosciences*, 44(1):1–26, 2012. doi: 10.1007/s11004-011-9376-z. cited By 249.
- [34] J. Caers. *Modeling Uncertainty in the Earth Sciences*. 2011. doi: 10.1002/9781119995920.
- [35] Y. Chen and D.S. Oliver. Cross-covariances and localization for enkf in multiphase flow data assimilation. *Computational Geosciences*, 14(4):579–601, 2010. doi: 10.1007/s10596-009-9174-6.
- [36] J. Rafiee and A.C. Reynolds. Theoretical and efficient practical procedures for the generation of inflation factors for es-mds. *Inverse Problems*, 33(11), 2017. doi: 10.1088/1361-6420/aa8cb2. cited By 38.
- [37] Catherine M.R. Yonkofski, Jason A. Gastelum, Ellen A. Porter, Luke R. Rodriguez, Diana H. Bacon, and Christopher F. Brown. An optimization approach to design monitoring schemes for co2 leakage detection. *International Journal of Greenhouse Gas Control*, 47:233–239, 4 2016. ISSN 17505836. doi: 10.1016/j.ijggc.2016.01.040.
- [38] S. Oladyshkin, H. Class, and W. Nowak. Bayesian updating via bootstrap filtering combined with data-driven polynomial chaos expansions: Methodology and application to history matching for carbon dioxide storage in geological formations. *Computational Geosciences*, 17(4): 671–687, 2013. doi: 10.1007/s10596-013-9350-6. cited By 36.
- [39] Mingliang Liu and Dario Grana. Petrophysical characterization of deep saline aquifers for co2 storage using ensemble smoother and deep convolutional autoencoder. *Advances in Water Resources*, 142, 8 2020. ISSN 03091708. doi: 10.1016/j.advwatres.2020.103634.
- [40] Mohamed Mehana, Bailian Chen, and Rajesh Pawar. Reduced-order models for wellbore leakage from depleted reservoirs. Unconventional Resources Technology Conference (URTEC), 2022. doi: 10.15530/urtec-2022-3725868.
- [41] Rajesh Pawar, Shaoping Chu, Bill Carey, David Tu, Nathan Moodie, Bailian Chen, and William Ampomah. Quantitative risk assessment of leakage through legacy wells in support of permit application for a large-scale co2 injection project in southwestern us, 2022.
- [42] Bailian Chen, Dylan R. Harp, Youzuo Lin, Elizabeth H. Keating, and Rajesh J. Pawar. Geologic co2 sequestration monitoring design: A machine learning and uncertainty quantification based approach. *Applied Energy*, 225:332–345, 9 2018. ISSN 03062619. doi: 10.1016/j.apenergy.2018.05.044.
- [43] J.H. Friedman. Multivariate adaptive regression splines. *Annals of Statistics*, 19(1):1–141, 1991.
- [44] D.H. Le and A.C. Reynolds. Optimal choice of a surveillance operation using information theory. *Computational Geosciences*, 18(3-4): 505–518, 2014. doi: 10.1007/s10596-014-9401-7.
- [45] J. C. Helton and F. J. Davis. Latin hypercube sampling and the propagation of uncertainty in analyses of complex systems. *Reliability Engineering & System Safety*, 81(1):23–69, 7 2003. ISSN 0951-8320. doi: 10.1016/S0951-8320(03)00058-9.
- [46] G.A. Zyvoloski, B.A. Robinson, Z.V. Dash, and L.L. Trease. Summary of the models and methods for the fehm application - a finite-element heat- and mass-transfer code. *Rep. LA-13307-MS*, 1997. cited By 165.
- [47] François Chollet et al. Keras. <https://keras.io>, 2015.
- [48] J. Caers. *Petroleum Geostatistics*, 2005. cited By 186.
- [49] B. Chen and A.C. Reynolds. Optimal control of icv's and well operating conditions for the water-alternating-gas injection process. *Journal of Petroleum Science and Engineering*, 149:623–640, 2017. doi: 10.1016/j.petrol.2016.11.004.
- [50] D. George, A. Kuprat, N. Carlson, and C. Gable. *LaGrIT - Los Alamos Grid Toolbox*, 1999. cited By 6.
- [51] S. Geisser. *Predictive Inference: An Introduction*, 1993.
- [52] Y. Xu and R. Goodacre. On splitting training and validation set: A comparative study of cross-validation, bootstrap and systematic sampling for estimating the generalization performance of supervised learning. *Journal of Analysis and Testing*, 2(3):249–262, 2018. cited By 311.
- [53] A. Chadwick, R. Arts, O. Eiken, P. Williamson, and G. Williams. Geophysical monitoring of the co2 plume at sleipner, north sea. *Advances in the Geological Storage of Carbon Dioxide*, pages 303–314, 2006. cited By 69.
- [54] Diana Koschel, Jean-Yves Coxam, Laurence Rodier, and Vladimir Majer. Enthalpy and solubility data of co2 in water and nacl (aq) at conditions of interest for geological sequestration. *Fluid phase equilibria*, 247(1-2):107–120, 2006.